International Journal of Microwave and Wireless Technologies

cambridge.org/mrf

A multiband truncated patch antenna based on EBG structure for IoMT and 5G networks

Saurabh Raj, Piyush Kumar Mishra and Vijay Shanker Tripathi

Department of Electronics and Communication Engineering, Motilal Nehru National Institute of Technology, Allahabad, Prayagraj, India

Research Paper

Cite this article: Raj S, Mishra PK, Tripathi VS (2023). A multiband truncated patch antenna based on EBG structure for IoMT and 5G networks. *International Journal of Microwave and Wireless Technologies* **15**, 1745–1757. https://doi.org/10.1017/S1759078723000454

Received: 20 April 2022
Revised: 28 March 2023
Accepted: 29 March 2023

Keywords:
5G network; circular polarization; electromagnetic band gap; Internet of Medical Things; millimeter-wave; multiband

Corresponding author:
Saurabh Raj,
Email: saurabhraj@mnnit.ac.in

Abstract

In this paper, a truncated patch antenna based on the electromagnetic band gap (EBG) structure has been proposed. The fabricated antenna has five operating frequencies at 10.4, 15.68, 19.68, 27.2, and 35.04 GHz. The fabricated prototype of the antenna constitutes a truncated rectangular patch etched with the shape of a symmetrical slot (on top) and an EBG loaded on the ground plane of the dielectric substrate. The optimized volume of the antenna is $20 \times 15 \times 1.57$ mm^3. The proposed antenna gives a good radiation pattern for the E-H field in all covered bandwidth and also achieved better performances related to the reference papers. A multiband antenna also covered the 5 G bandwidth, which resonates at 27.2 GHz from 24.2 GHz to 27.84 GHz bandwidth and at 35.04 GHz from 33.84 GHz to 36.2 GHz bandwidth, which can be used in the Internet of Medical Things. On the other hand, X/Ku/K frequency bands have been committed for wireless communication where the multiband antenna can be used to help in monitoring, especially in the case of data transmission from radio frequency sensors to health-care system in real-time applications.

Introduction

Recently, research in the Internet of Medical Things (IoMT) is gaining attention as a resource for enhancement in medical diagnosis, treatment, and biotelemetry purposes. Nowadays, various IoMT-based devices are being developed for different applications such as noninvasive blood glucose monitoring, blood pressure measurement, heart rate monitoring, insulin pumps, tumor detection, and endoscopy. Currently, 5 G networks are being deployed in many countries. It has potential application for communicating diagnostic reports like high or low blood pressure, glucose level in blood plasma, body temperature, and heart rate. 5 G networks can also be used to implement telemedicine systems efficiently. A multiband antenna can be inserted into the patient's body or attached over the upper body part to make a biotelemetry system along with medical devices such as biosensors, routers, micro-base stations, and a wide area network for IoMT applications. Diagnostic reports like glucose level in the blood, blood pressure, and heart rate from a radio frequency (RF) sensor imbedded in the human body or wearable on the body can be wirelessly transferred to smart health-care systems [1]. IoMT-enabled devices can make health-care affordable and approachable for all. It has developed the feature of health care by giving dynamic nature in real-time approach [2]. It supports the patients to take suitable measures in case of serious illness conditions like high and low glucose concentration in blood, high and low blood pressure, brain tumor, and cardiac attack [3]. It eases remote sensing check-up facility that reduces the costs. The IoMT has an important role to transform the health-care systems and minimize the cost of medical devices such as RF sensor that provides different bands by using a single antenna. Many wearable medical devices for IoMT and 5 G networks applications in smart health-care structures are being developed, such as RF sensors for noninvasive blood glucose level monitoring, pacemaker for cardiac disease, and diagnostic of brain tumor. In near future, 5 G networks will support operation of the IoMT [4]. IoMT applications in the 5 G spectrum will result in the development of a smart health-care system [5]. The smart health-care system and its main components are depicted in Fig. 1, which is based on the 5 G network.

Advanced medical devices in smart health-care systems are based on many novel ideas of research for implantable and wearable RF sensors [6]. A wearable medical device such as an RF sensor can have noninvasive monitoring in real-time mode. It can transmit diagnostic information like blood glucose levels, high blood pressure, brain stroke, and cardiac attack to the health-care system, where medical experts are ready for the treatment of patients [7]. An RF sensor is attached in or around the body part to establish a Wireless Body Area Network (WBAN) [8]. The advantages of RF/microwave frequency bands are being utilized in IoMT, wireless communications, satellite communications, and 5 G network applications. By using multiband antenna design, handy medical diagnostic tools like RF sensors for glucose level monitoring and heart rate monitoring devices are also developed. In tumor detection

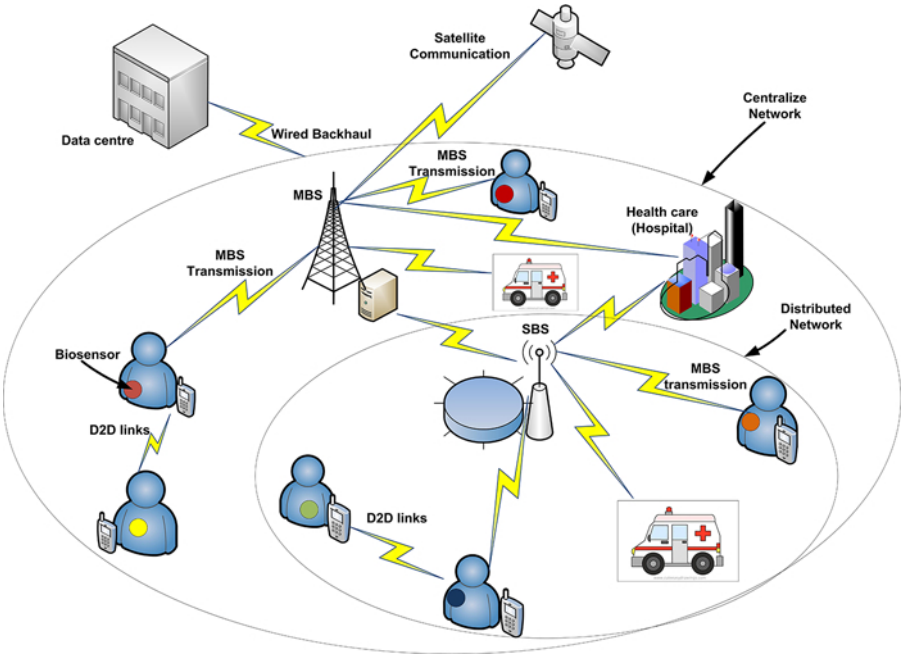

Figure 1. Schematic view of smart health-care system based on a 5 G network [2].

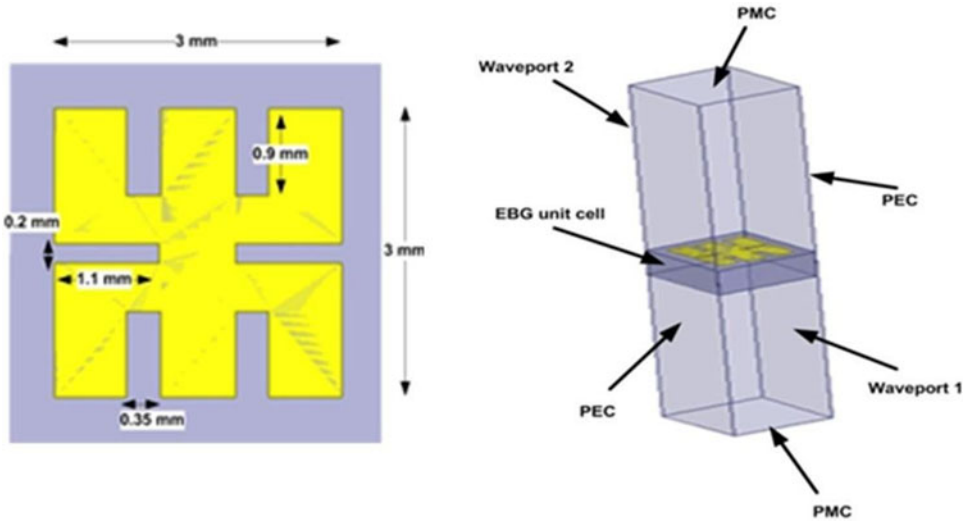

Figure 2. EBG structure of ground plane unit cell.

systems based on microwave/RF bands, a multiband antenna is used in the wide super-high frequency (SHF) band from 0.5 to 40 GHz for the low depth of access inside human tissues. Development in implantable/wearable technology has resulted in the new design of RF sensors for medical applications such as glucose monitoring [9, 10], neural recording [11], intracranial pressure monitoring [12, 13], and endoscopy [14, 15]. The key element of a health-care system is an RF sensor, which is used for communicating the RF signal in between the RF sensor and health-care systems [16, 17]. Human tissues are lossy medium for RF/Electro Magnetic (EM) waves, and some of the RF waves are absorbed within human tissues [18]. A novel design of the antenna is needed, which contains low backward radiations and minimum Specific Absorption Rate (SAR) value that results in less harm to the human tissues [19]. Biomedical devices are wireless devices; they have a single antenna with multiple band, RF sensors, a transmitter, and a microcontroller unit, which can be attached to the patient's body or etched on clothing [20]. It has many issues related to RF sensors design. The design of a flexible antenna with stable characteristics and specified limits of the SAR value are important issues [21–24]. Design should be compact in size, and it should be smart enough that it can operate in different spectrum using a single antenna design. Multiband designs substitute the application of conventional patch antennas for different resonant frequencies [25–27]. The multiband antenna can be designed by unique geometric variation, such as slot cuts on patch and structures on ground plane are the important components in conventional microstrip patch antennas. Recently, several methods to obtain multiband antennas such as subtracting the slots on the patch [28] and loading of metamaterial-based configurations [29, 30] on the radiating patch are being used. Defective ground structures (DGS) can also be used on the ground plane to cover the multiple bands by a single antenna design. A multiband antenna is designed that covers SHF satellite communication applications [31]. A rectangle-shaped

https://doi.org/10.1017/S1759078723000454 Published online by Cambridge University Press

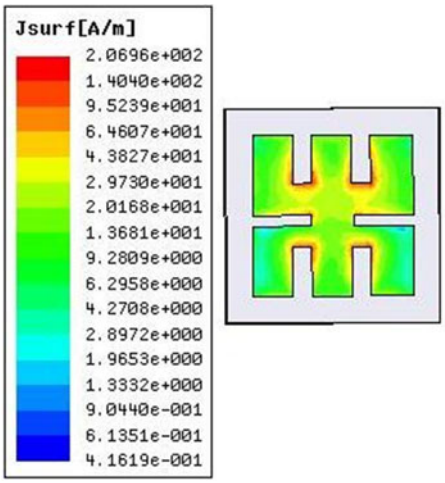

Figure 3. Current distribution on EBG unit cell.

microstrip patch antenna has been developed to function at a wide range of frequencies, including those used in Intelligent Transport System (ITS) and satellite communications applications [32]. In [32], a compact antenna is designed for use of ground mobile satellite communications for vehicles. In [33], a square slotted patch is designed for dual-band satellite communication applications. In [34], a monopole antenna having dual-band notch is designed, which is used in satellite communication for X/Ku-band applications. In [35], a fractal patch antenna is designed for SHF satellite communication. In [36], a metamaterial-based miniaturized patch antenna is designed for satellite communication, GPS, and Wireless Local Area Network (WLAN) applications. In [37], a DGS-based ultra-wideband antenna is designed for WLAN applications. A slotted patch antenna that operates in the Ku-band is reported in [38]. An oval-shaped ring patch antenna is shown in [39]. The antenna described in this study is efficient, has a good impedance bandwidth, and is suited for C/X/Ku/K band satellite communications. In [40], an elliptical ring patch multiband antenna is reported.

A multiband antenna that covers multiple frequency bands, such as C/X/Ku/K wireless communication, is designed in [41]. In [42], a poly fractal shape microstrip patch antenna with circularly polarized multiband is proposed. In [43], a triband antenna is proposed. It has achieved circular polarization at multiple resonant frequencies for Bluetooth, WLAN, and ITS applications. The manufactured dipole antenna in [44] is mounted to a dielectric substrate that possesses the same electrical properties as human tissue. It is shown that nanomaterial is an ideal material for SAR minimization. For the biotelemetry system, a compact dual-band circular patch antenna is constructed in [45]. The designed antenna covers Industrial Scientific and Medical bands (ISM), Medical Implantable Communication System (MICS), and Med Radio for biomedical applications [45]. For Radio Frequency Identification (RFID) biomedical applications, a small, circularly polarized implanted antenna is developed [46]. An RFID antenna for in body measurement is developed in [46]. In [47], a small antenna loaded on a superstrate is designed for biomedical applications in the ISM band. In [47], an antenna with a small volume of $(25 \times 25 \times 1.92)$ mm^3 was proposed, which is developed for biomedical telemetry applications. An extremely tiny implanted antenna for biomedical applications is reported in [48]. The antenna is fabricated on Roger RO3003 ($\varepsilon_r = 3$) with an overall volume of $5 \times 5 \times 0.26$ mm^3. The designed antenna operates at a 2.45 GHz resonant frequency with 460 MHz impedance bandwidth and a gain of −22.6 dB observed in human body. The ISM band is used by a circularly polarized implanted patch antenna for biomedical applications [49]. The proposed antenna has a compact dimension of 10 mm × 10 mm × 0.5 mm. A novel compact-size implantable circular antenna is proposed in [50]. It provides wireless information and energy transmission at the ISM and Medical Device Radio-communication bands.

The multiband antenna operates in multiple bands, which can be used for IoMT and 5 G applications. In this paper, the discussion about a multiband antenna for IoMT and 5 G networks is divided into five sections. The first section describes the introduction of a literature survey on multiband antenna for biomedical applications. The second section states the methodology of electromagnetic band gap (EBG) structure design on radiating patch antenna. In the third section, antenna design parameters are discussed. In the fourth section, results are discussed. Finally, the conclusion is given in the fifth section.

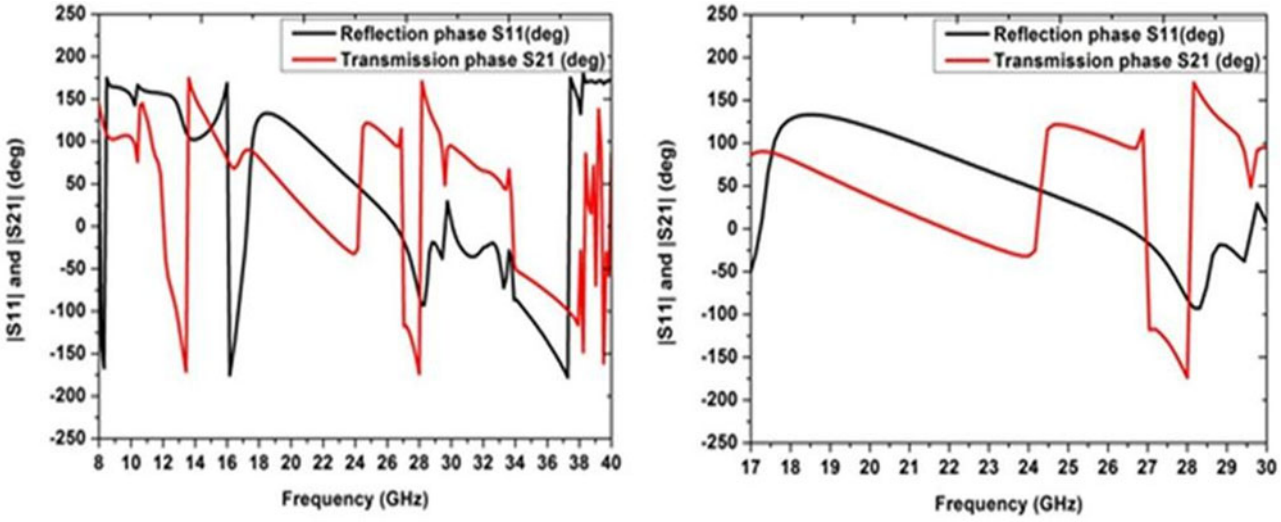

Figure 4. Band gap of EBG surface with the reflection phase diagram.

https://doi.org/10.1017/S1759078723000454 Published online by Cambridge University Press

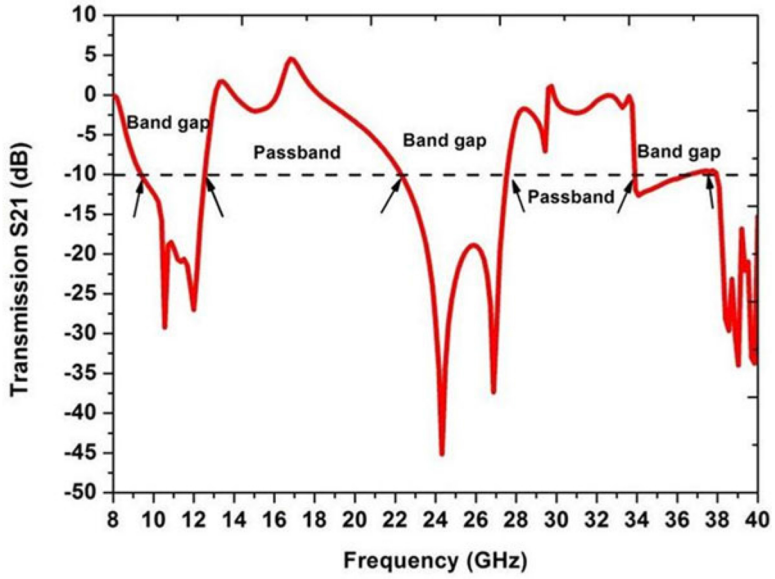

Figure 5. Band gap of EBG surface with transmission loss graph.

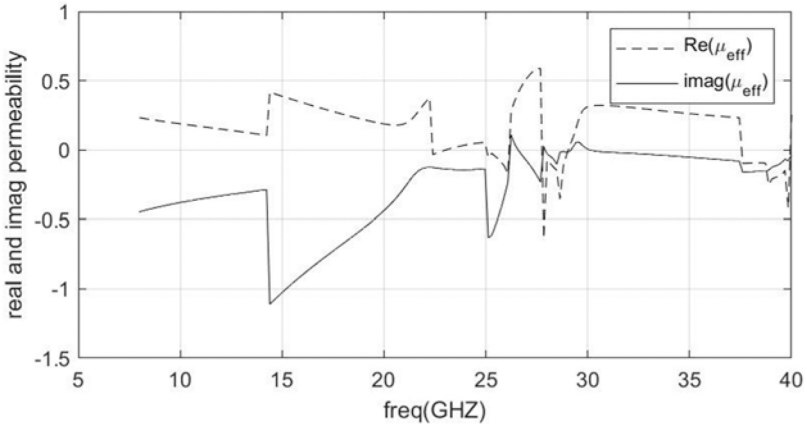

Figure 6. Real and Imaginary permeability of design unit cell.

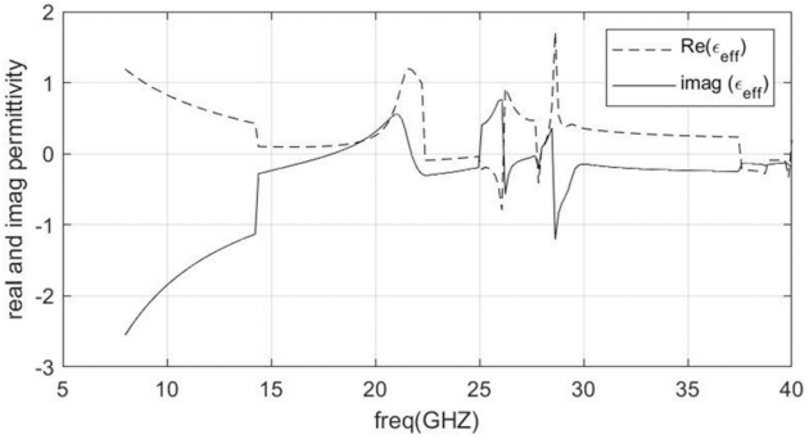

Figure 7. Real and Imaginary permittivity of design unit cell.

Electromagnetic band gap structure design methodology

In Fig. 2, a unit cell of the EBG structure with the dimensions 3×3 mm^2 is depicted. The periodic arrangement of EBG on the ground plane has been realized from the dispersion graph, the reflection phase, and the transmission loss parameters. The current distribution on EBG unit cell is illustrated in Fig. 3. The slit gap of the unit cell construction is the location where the maximum current density is obtained, as can be seen in this figure. This results in a $\pm 180^{\circ}$ reflection phase at a particular frequency range.

By using a reflection phase graph, an electromagnetic property has been determined in Fig. 4. The reflection phase of 180° shows a Perfect Electric Conductor (PEC) and reflection phase of 0° implies a perfect magnetic conductor (PMC) plane.

https://doi.org/10.1017/S1759078723000454 Published online by Cambridge University Press

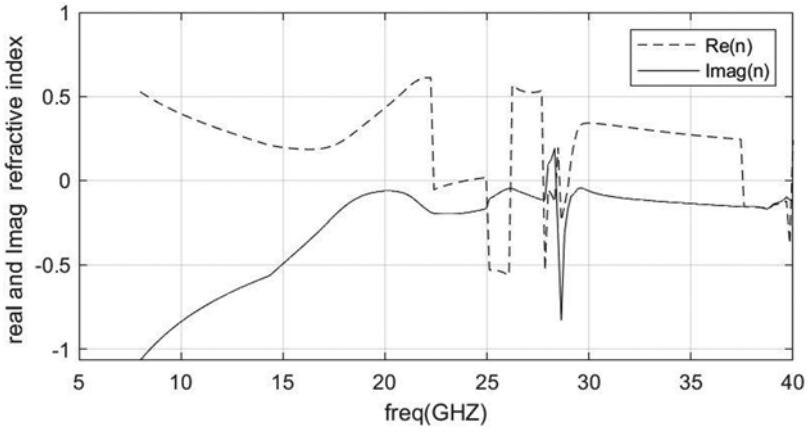

Figure 8. Real and Imaginary refractive index of design unit cell.

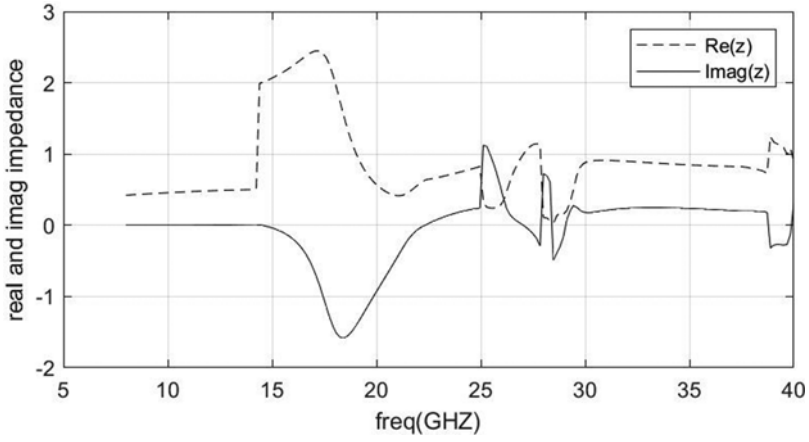

Figure 9. Real and imaginary impedance of design unit cell.

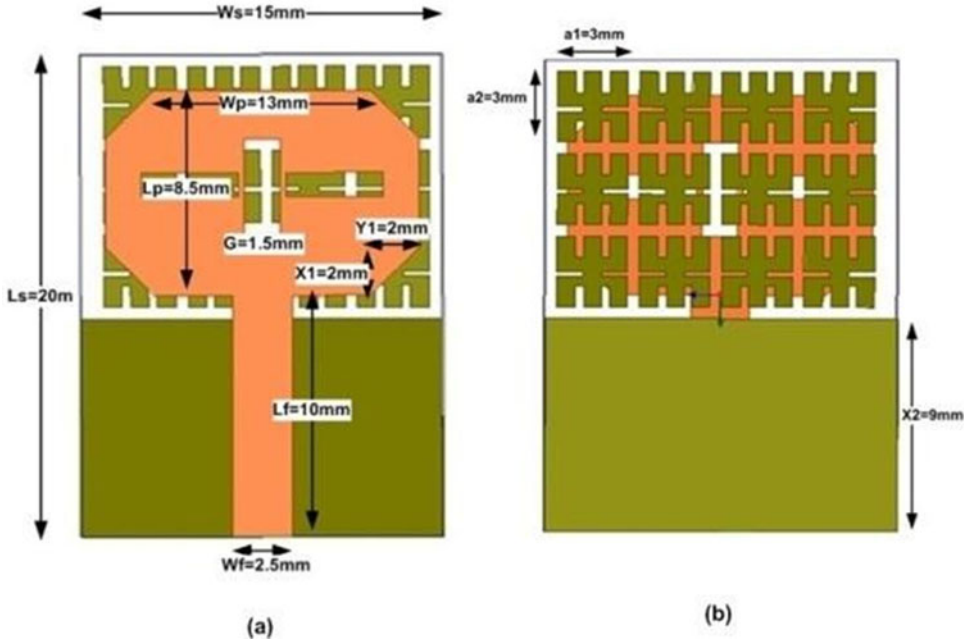

Figure 10. The simulated geometry of the proposed EBG-based truncated patch antenna: (a) top view and (b) bottom view.

In nature, the PMC does not exist. An EBG structure plane has reflection phase changes from +180° to −180° by increasing frequency [51].

The bandwidth of frequency from +90° to −90° in the reflection phase variation matches with the bandgap of the EBG ground plane unit cell. The reflection phase diagram within a particular

https://doi.org/10.1017/S1759078723000454 Published online by Cambridge University Press

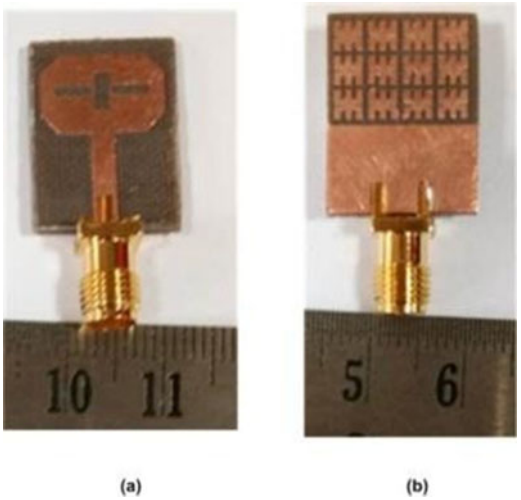

Figure 11. The fabricated design of the proposed EBG-based truncated patch antenna: (a) top view and (b) bottom view.

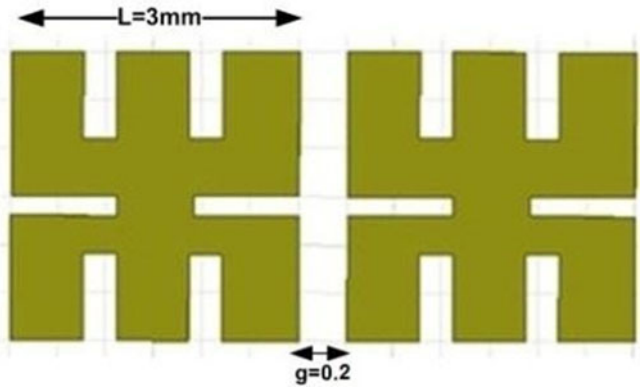

Figure 12. Planner periodic EBG structure.

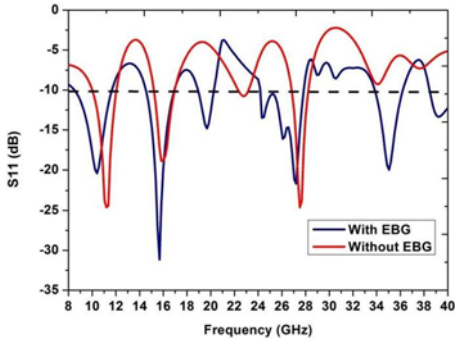

Figure 13. Simulated reflection coefficient S_{11} (dB) versus frequency with and without EBG.

frequency range is shown in Fig. 4. As shown in Fig. 5, a multiple band of the frequency with transmission loss S_{21} of <-10 dB is typically measured as the band gap [52, 53].

In Figs. 6 and 7, the artificial material parameters such as effective permeability and effective permittivity are shown. These graphs shows that both negative permeability and permittivity bands lie between approximately 25 and 26 GHz, 27 and 29 GHz, and 37 and 40 GHz. This result implies that these particular

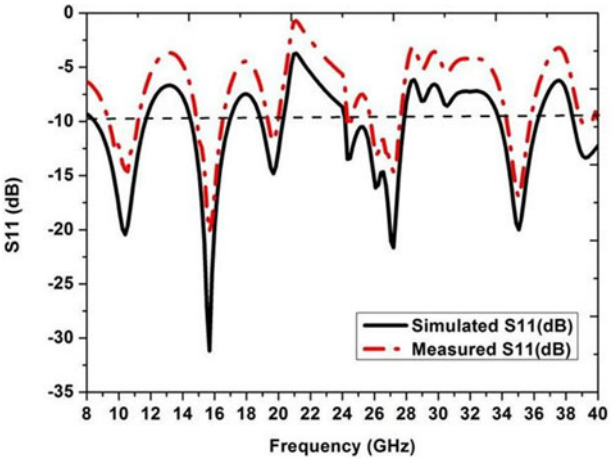

Figure 14. Simulated and measured graph of S_{11} (dB) with EBG.

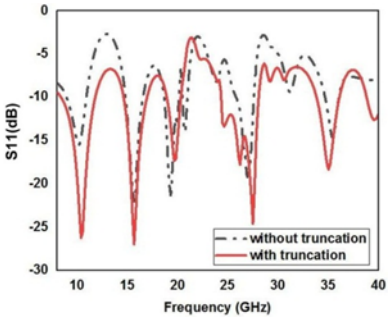

Figure 15. S_{11} graph with and without truncation on the corner of a rectangular patch.

frequency bands of design unit cell work as an EBG structure. As a result, incident waves experience a zero degree reflection phase shift. Planner periodic structure array has been used on ground plane for surface wave reduction.

According to [54], a metamaterial with symmetrical geometry's effective thickness (d) is measured (in the plane of EM propagation). When the measurement locations are situated close to the periodic arrangement of metamaterial, undesirable modes of higher order are produced, which results in improper effective permittivity and permeability. To get precise S-parameters, the observation nodes must be placed far enough from the metamaterial surface to achieve the dominant mode. The wave impedance and the refractive index in [54], electromagnetic wave with normal incidence on a homogeneous surface, have the following correlations with the S-parameters:

$$S_{11} = \frac{R_{01}\left(1 - e^{i2N_{\text{eff}}k_0 d}\right)}{\left(1 - R_{01}^2 e^{i2N_{\text{eff}}k_0 d}\right)} \tag{1}$$

$$S_{11} = \frac{\left(1 - R_{01}^2\right)\left(e^{i2N_{\text{eff}}k_0 d}\right)}{\left(1 - R_{01}^2 e^{i2N_{\text{eff}}k_0 d}\right)} \tag{2}$$

$$R_{01} = \frac{Z_{\text{eff}} - 1}{Z_{\text{eff}} + 1}, \tag{3}$$

where $N_{\text{eff}}(\omega) = n_{\text{eff}} + k_{\text{eff}}$ denotes the complex refractive index, Z_{eff} denotes the complex impedance of wave, n_{eff} denotes the effective refractive index, k_{eff} is the effective extinction coefficient, k_0 denotes the wave number, and ω denotes as the angular frequency.

https://doi.org/10.1017/S1759078723000454 Published online by Cambridge University Press

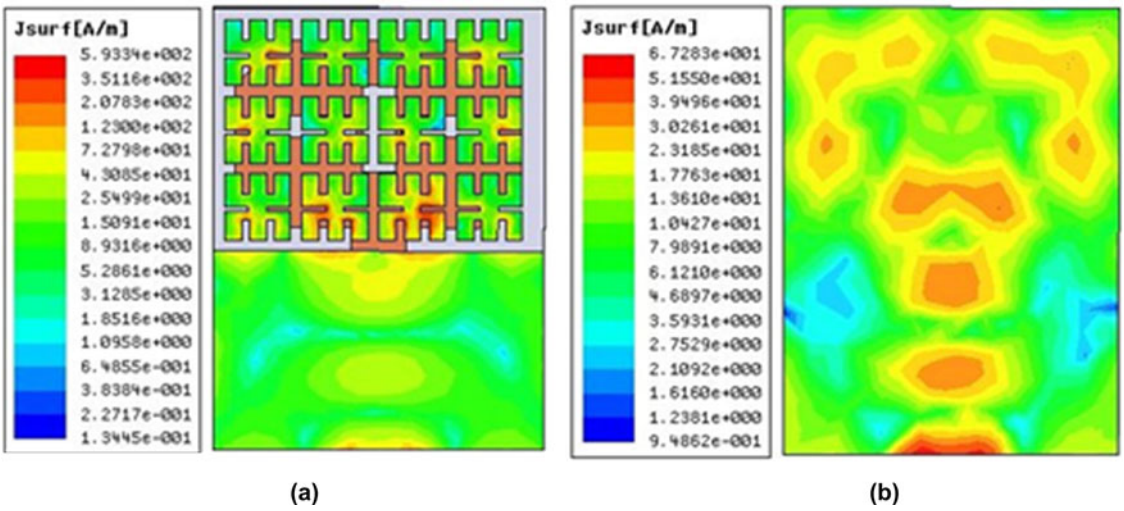

Figure 16. Surface current density (a) with EBG and (b) with PEC.

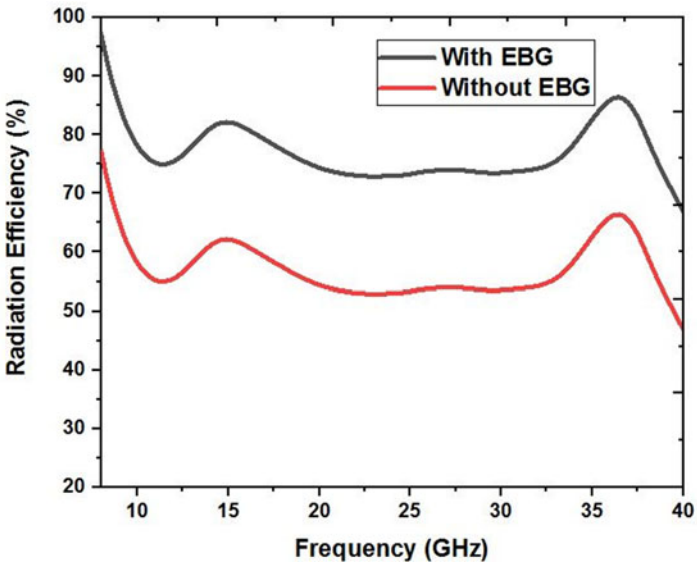

Figure 17. Radiation efficiency graph with and without loading of EBG ground plane.

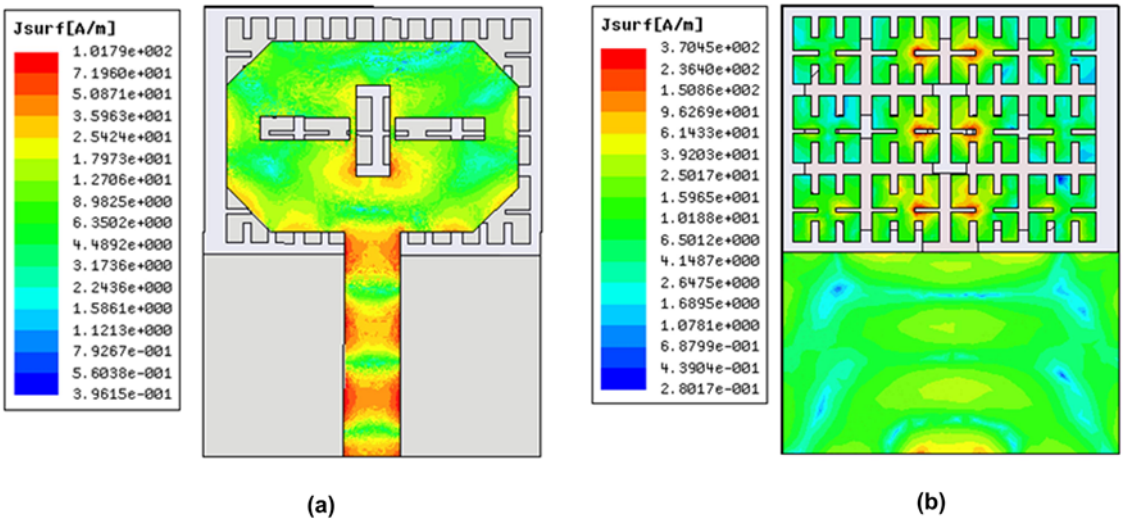

Figure 18. Surface current distribution (a) on radiating patch and (b) on EBG ground plane.

https://doi.org/10.1017/S1759078723000454 Published online by Cambridge University Press

A unique method for determining metamaterial parameters is proposed, which is based on the Kramers–Kronig correlation. Effectively using equations (4) and (5) in the case of a uniform substrate with properly specified substrate boundaries and known *S*-parameters is proposed. Once the thickness of the homogeneous substrate has been defined and the material's properties are known, it is possible to calculate the *S*-properties using the analytical formulas (1) and (2). The effective magnetic permeability and effective electric permittivity are determined using the effective material parameter extraction algorithm.

Effective impedance (Z_{eff}) parameter has been calculated from the values achieved from the waveguide medium as [54],

$$Z_{\text{eff}} = \pm\sqrt{\frac{(1+S_{11}^2)-S_{21}^2}{(1-S_{11}^2)-S_{21}^2}}, \tag{4}$$

$$e^{i2N_{\text{eff}}k_0 d} = \frac{S_{21}}{1-S_{11}R_{01}}. \tag{5}$$

From this value of effective impedance (Z_{eff}), effective permeability (μ_{eff}), effective permittivity (ε_{eff}), and refractive index (N_{eff}) are calculated by following equations [54, 55]:

$$\mu_{\text{eff}} = N_{\text{eff}} \times Z_{\text{eff}}, \tag{6}$$

$$\varepsilon_{\text{eff}} = \frac{N_{\text{eff}}}{Z_{\text{eff}}}, \tag{7}$$

$$n_{\text{eff}} = \frac{1}{k_0.d}\left\{I_{\text{m}}\left[\left(\ln e^{ink_0 d}\right)\right] + 2m\pi - R_{\text{e}}\left[\ln e^{ink_0 d}\right]\right\}. \tag{8}$$

By equations (6)–(8), the complete values of μ_{eff}, ε_{eff}, and n_{eff} have been calculated using MATLAB code. These values are shown in Figs. 6–8, respectively. It can be observed that the value of effective permeability, effective permittivity and refractive index are negative between bandwidth of 25 to 26 GHz, 27 to 29 GHz, and 37 to 40 GHz, respectively. At this particular frequency band, the stop band phenomena is seen for designed unit cell of EBG structure.

In Fig. 9, the impedance magnitude of the designed unit cell of EBG is shown. It is found to be positive throughout the frequency bandwidth, which implies that a high impedance surface has been achieved. It has high impedance surface for both TE and TM polarization, and this results in minimum surface wave propagation at particular frequency bandwidth. Moreover, the band gap property of EBG for surface wave reduction enhances the peak gain of antenna, minimizes the backward wave propagation, and decreases mutual coupling.

Antenna design and its specification

In this work, an EBG-based truncated patch antenna is simulated, which is illustrated in Fig. 10. The geometry of the truncated patch is designed on the RT/Duroid dielectric substrate with a dielectric constant (ε_r) of 2.2, with the height of 1.57 mm, which is depicted in Fig. 10(a). The developed antenna, depicted in Fig. 10(b), has an EBG structure loaded in the ground plane to reduce surface current and improve radiation properties like impedance bandwidth, realized gain, and antenna efficiency. By using HFSS v18 simulation software, the dimensions depicted in Fig. 10 have been optimized. A conventional microstrip line with 50 ohms SMA connector is used for feeding RF power. Fig. 11 displays the lab-fabricated prototype of an antenna. The optimized volume of the fabricated antenna is $20 \times 15 \times 1.57$ mm^3. Due to truncation on the corner of a rectangular patch with slot subtract on radiating patch, a good impedance matching has been obtained with the transmission line. The slot is cut of rectangular shape on the radiating patch in a symmetrical manner, which produces capacitive coupling with the periodic structure of EBG on the bottom of the substrate. It reduces current density on the surface of the dielectric substrate, which leads to maximum power radiation in free space.

The gaps between EBG unit cells usually have a very high aspect ratio, and as a result, it introduces a high coupling effect in a capacitor that miniaturized the physical size of the antenna, which is illustrated in Fig. 12. The use of planner periodic EBG structure loading on the ground has led to the propagation of TM0 in planner structure. Due to TM0 propagation, the surface current in the substrate is reduced [56].

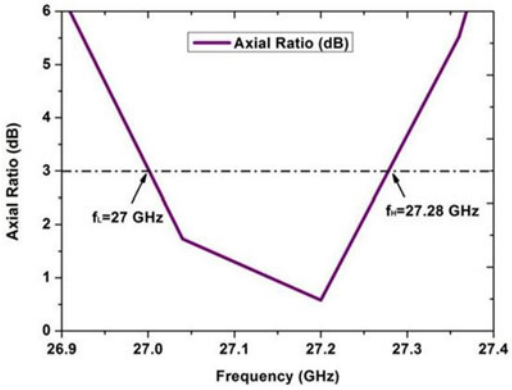

Figure 19. Simulated result of axial ratio at 27.2 GHz.

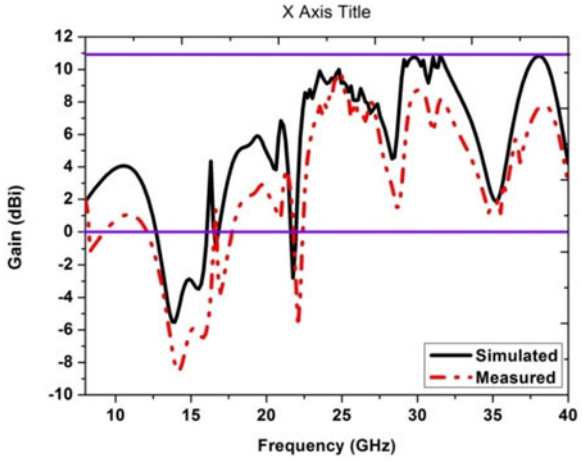

Figure 20. Simulated and measured gain of proposed antenna at multiple resonant frequencies.

Results and discussion

HFSS v18 is used for the simulation of an optimized antenna. First, the patch antenna without loading of EBG structure is simulated in the HFSS tool. The simulated graph of reflection coefficient S_{11} (dB) with and without loading of periodic EBG ground structure is shown in Fig. 13. The graph shows that due to the stacking of the periodic structure of EBG on the ground plane, two more bands are available for communication, and impedance matching is improved compared to without loading EBG structure. A good agreement is achieved in the simulated and measured graph of

https://doi.org/10.1017/S1759078723000454 Published online by Cambridge University Press

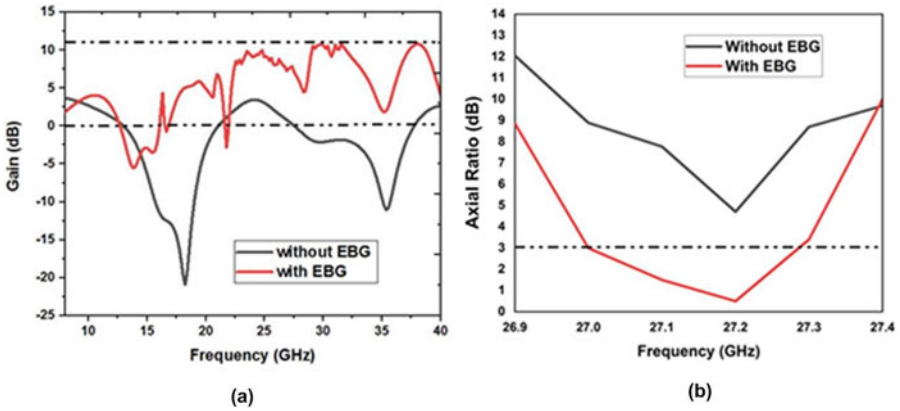

Figure 21. (a) Gain of antenna with and without EBG and (b) axial ratio of antenna with and without EBG.

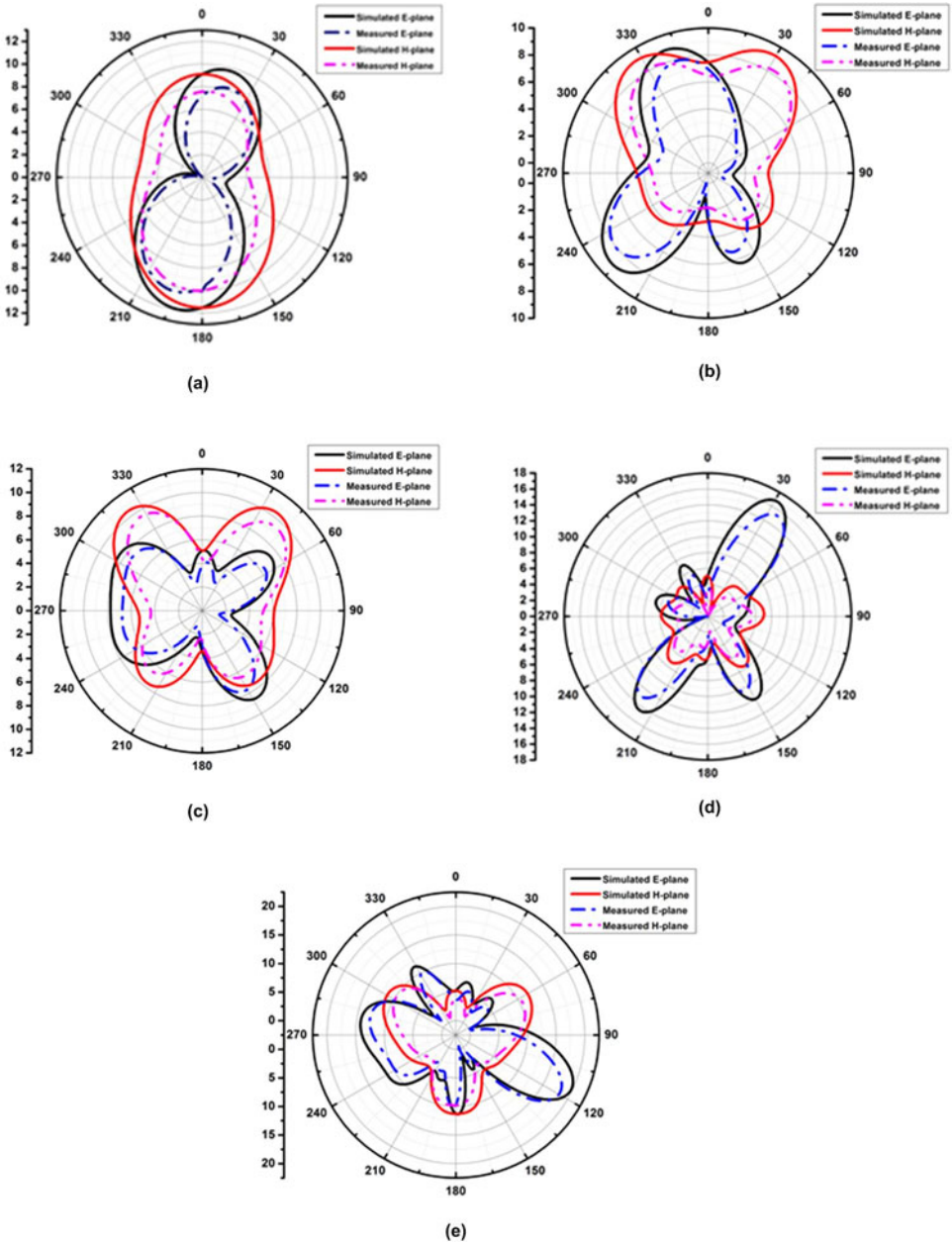

Figure 22. Simulated and measured radiation pattern at (a) 10.4 GHz, (b) 15.68 GHz, (c) 19.68 GHz, (d) 27.2 GHz, and (e) 35.04 GHz.

https://doi.org/10.1017/S1759078723000454 Published online by Cambridge University Press

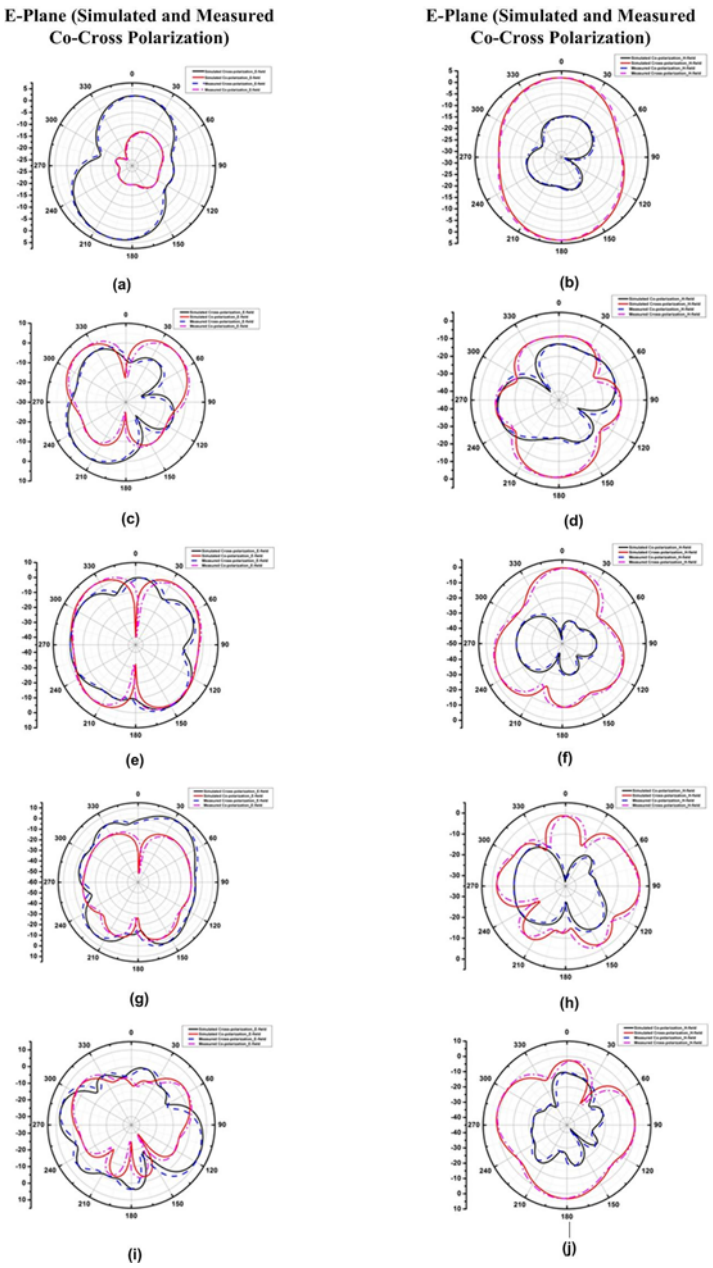

Figure 23. Simulated and measured co-cross-polarization in E- and H-planes (dB) at (a) and (b) 10.4 GHz, (c) and (d) 15.68 GHz, (e) and (f) 19.68 GHz, (g) and (h) 27.2 GHz, and (i) and (j) 35.04 GHz.

S_{11} (dB), which is shown in Fig. 14. Truncated patch antenna with the loading of EBG ground plane are resonating at five different resonant frequencies of 10.4 GHz (BW: 8.5 to 11.66 GHz), 15.68 GHz (BW: 14.5 to 16.9 GHz), 19.68 GHz (BW: 18.9 to 20.3 GHz), 27.2 GHz (BW: 24.2 to 27.84 GHz), and 35.04 GHz (BW: 33.84 to 36.2 GHz), which covers X/Ku/K/Ka/mm-wave bands, respectively. A good impedance matching is obtained with the feed line due to the truncated corner and slot cut on the patch that produces multiple resonant frequencies.

The simulated result of radiating patch with and without truncation on the corner of rectangular patch is shown in Fig. 15. It shows that due to truncation on the corner of the rectangular patch, the impedance matching has improved and bandwidth has also been enhanced.

Due to the loading of the periodic structure with a 3 × 4 EBG array on the bottommost of the dielectric substrate, the back lobe is reduced, and a 180° phase shift occurs in the frequency band gap, enhancing the antenna performance. Figure 16 shows the surface current density on the EBG-loaded ground plane and PEC-loaded ground plane at the resonant frequency. The surface current is reduced by loading the EBG structure because of its frequency band gap. Because of the EBG structure's high impedance and reduced surface wave propagation in the ground plane, the resonant frequency is in the band gap region. It demonstrates that the radiation from the designed antenna has enhanced in the intended direction.

Due to the loading of the EBG structure on the ground plane, the radiation efficiency is enhanced, which is shown in Fig. 17. It is observed that by loading of the EBG ground plane, the average radiation efficiency increases from 55% to 75%.

Figure 18 shows the current distribution on the radiating patch and EBG ground plane. It implies that the transmission line and

https://doi.org/10.1017/S1759078723000454 Published online by Cambridge University Press

Figure 24. Measurement setup for glucose level monitoring by loading of thumb on radiating patch.

edges of the rectangular slot have a maximum current density, which leads to good impedance matching in multiple bands of frequencies. On the other hand, the current distribution on EBG-loaded ground plane shows maximum current flow along the radiating patch, which leads to good impedance matching with the transmission line and reduces surface wave on the dielectric substrate. In the proposed antenna design, circular polarization is obtained at the resonant frequency of 27.2 GHz ranging from 27 to 27.28 GHz, which is illustrated in Fig. 19. The designed antenna has an axial ratio of <3 dB, which shows the circular polarization. A circularly polarized antenna radiates EM waves in every dimension, which is required for receiving data at the receiver point. The realized peak gain of the fabricated antenna concerning frequency is illustrated in Fig. 20. In Fig. 20, the antenna shows a maximum peak gain of 4, −4, 6, 8.5, and 2.5 dBi at 10.4, 15.68, 19.68, 27.2, and 35.04 GHz resonant frequencies, respectively.

Figure 21(a) and (b) shows that by loading EBG on the ground plane, the gain of the antenna has improved from 2 to 8.5 dB at 27.2 GHz resonant frequency and the axial ratio also improved, which achieves the circular polarization from 27 to 27.28 GHz frequency band.

In Fig. 22, radiation pattern at multiple resonant frequencies are shown. The magnitude of electric field intensity on radiating patch in the field plot implies that the proposed antenna is working at multiple resonant frequencies. It shows that the truncated point in the rectangular patch has maximum radiation intensity. The radiation pattern shows that the proposed antenna is a directional antenna that can be used for point-to-point wireless communication including long-range connectivity applications between two devices.

Polarization is the orientation of the electric field. Co-polarization is the desired polarization, and orthogonal to polarization is cross-polarization, which is undesired. The electric field of co-polarization defines the signal strength, and cross-polarization defines the undesired noise signal. Co- and cross-polarization in the E-plane and H-plane are shown in Fig. 23. It has been observed that approximately symmetric with some directionality, E-H field with low co-polarization magnitude has been realized in H-plane.

Table 1. Comparison of the parameter of proposed design with other referenced paper

Reference	Dimension	Resonant frequency (GHz)	Peak Gain (dBi)
[31]	8 × 16 mm^2	8.7, 16.4, 19.6	8.4, 8.04, 3.12
[32]	14 × 12 mm^2	4.96, 7.76, 12.72, 29.3	2.03 to 7.77
[33]	40 × 35 mm^2	13, 18	3.14 to 4.98 and 2.03 to 2.58
[34]	20 × 20 mm^2	4.5, 7, 9, 12, 15	6.96
[35]	15 × 15 mm^2	8.8, 10.8, 13.02, 15.23	1.56
[36]	24.6 × 22.15 mm^2	8.5, 17.7, 20, 23.7,30	9.6
[40]	50 × 50 mm^2	2.4, 3.4, 5.8	NA
[45]	340 mm^3 (volume)	4.3.5 MHz, 433.9 MHz and 2.45 GHz	4.8
[46]	$\pi \times (6)^2 \times 1.27$ mm^3	902–928 MHz	8.1
[47]	25 × 25 × 1.28 mm^3	915 MHz	NA
[57]	12 × 14 × 1.6 mm^3	5.72, 14.3, and 16.06 GHz	NA
[58]	$0.144\lambda_0 \times 0.105\lambda_0 \times 0.003\lambda_0$	820–990 MHz, 1.87–2.08 GHz, 2.37–2.93 GHz, 3.98–4.27 GHz, and 5.47–8.9 GHz	NA
[59]	$\pi \times (4)^2 \times 1.6$ mm^3	27.5–28.8 GHz, 32.45–34.65 GHz	NA
Proposed work	20 × 15 × 1.57 mm^3	10.4, 15.68, 19.68, 27.2, 35.04	4, −4, 6, 8.5, 2.5

It shows the radiation pattern in pass bands between multiband frequencies. The motive of the field pattern is to determine that the proposed design essentially covers a multi bandwidth. The electric field pattern is almost same as the pattern of the dipole antenna. The cross-polarization increases at a certain magnitude with higher frequencies due to a wide area of radiation. The cross-polarization is less than −10 dB in H-plane, which is desired for radiation purposes in wireless communication for biotelemetry applications.

The proposed antenna can be used as an RF sensor device for monitoring blood glucose levels non-invasively. Fig. 24 shows that by loading the thumb as a superstrate on top of the radiating patch, there is a remarkable frequency shift. This shift is measurable, and using a single-pole cole-cole model, the shift in resonant frequency can be used for calibrating glucose levels directly.

Finally, the proposed work is compared with other reference work as shown in Table 1. This shows that the proposed work gives better results than reference papers.

Conclusion

In this paper, an EBG ground structure-based truncated patch antenna has been proposed. It has a compact volume of

https://doi.org/10.1017/S1759078723000454 Published online by Cambridge University Press

$20 \times 15 \times 1.57$ mm^3. The proposed multiband antenna has a good gain over a wide frequency range. The designed antenna has average radiation efficiency of 75% throughout the wide frequency range. In the proposed antenna design, the current density on the surface is minimized due to the loading of electromagnetic bandgap at the bottom of the dielectric substrate. It results in maximum RF/EM radiation in free space. The designed truncated antenna has a peak gain of 8.5 dBi at 27.2 GHz resonant frequency. It covers 24.2 to 27.84 GHz bandwidth, which is allocated to 5 G networks. By loading the electromagnetic bandgap structure, the fundamental parameters of the microstrip patch antenna such as impedance matching, bandwidth, and radiation efficiency have been enhanced. The proposed design has a novel structure having multiple bands at 10.4 GHz for X-band, 15.68 GHz for Ku-band, 19.68 GHz for K-band, 27.2 GHz for Ka-band, and 35.04 GHz for the mm-Wave band. The designed multiband antenna can be used for telemetry applications in IoMT and 5 G networks, as well as disease detection and diagnostics in order to improve the health-care system.

Financial support. This research received no specific grant from any funding agency, commercial, or not-for-profit sectors.

Competing interests. The authors report no conflict of interest.

References

1. **Kaur G, Kaur A, Toor GK, Dhaliwal BS and Pattnaik SS** (2015) Antennas for biomedical applications. *Biomedical Engineering Letters* **5**, 203–212.
2. **Ahad A, Tahir M, Aman Sheikh M, Ahmed KI, Mughees A and Numani A** (2020) Technologies trend towards 5G network for smart health-care using IoT: A review. *Sensors* **20**, 4047.
3. **Sundaravadivel P, Kougianos E, Mohanty SP and Ganapathiraju MK** (2018) Everything you wanted to know about smart health care: Evaluating the different technologies and components of the internet of things for better health. *IEEE Consumer Electronics Magazine* **7**(1), 18–28.
4. **Liu X, Jia M, Zhang X and Lu W** (2019) A novel multichannel Internet of Things based on dynamic spectrum sharing in 5G communication. *IEEE Internet of Things Journal* **6**(4), 5962–5970.
5. **Li D** (2019) 5G and intelligence medicine—How the next generation of wireless technology will reconstruct healthcare? *Precision Clinical Medicine* **2**, 205–208.
6. **Amjadi M, Kyung K and Park I** (2016) Stretchable, skin-mountable, and wearable strain sensors and their potential applications. *Advanced Functional Materials* **26**(11), 1678–1698.
7. **Khan Y, Ostfeld AE, Lochner CM, Pierre A and Arias AC** (2016) Monitoring of vital signs with flexible and wearable medical devices. *Advanced Materials* **28**(22), 4373–4395.
8. **Cao H, Leung V, Chow C and Chan H** (2009) Enabling technologies for wireless body area networks: A survey and outlook. *IEEE Communications Magazine* **47**(12), 84–93.
9. **Powar Sharad V and Bombale UL** (2017) Antenna design for biomedical application. *International Journal of Engineering Research and Applications (IJERA)* **7**(11), 57–60.
10. **Liu LW, Kandwal A, Cheng Q, Shi H, Tobore I and Nie Z** (2019) Non-invasive blood glucose monitoring using a curved Goubau line. *Electronics* **8**, 662.
11. **Sharma A, Kampianakis E and Reynolds MS** (2017) A dual-band HF and UHF antenna system for implanted neural recording and stimulation devices. *IEEE Antennas and Wireless Propagation Letters* **16**, 493–496.
12. **Shah SAA and Yoo H** (2018) Scalp-implantable antenna systems for intracranial pressure monitoring. *IEEE Transactions on Antennas and Propagation* **66**(4), 2170–2173.
13. **Khan MWA, Khan A, Rizwan M, Sydänheimo L, Björninen T, Ukkonen L and Rahmat-Samii Y** (2018) Loop antenna for deep implant powering in an intracranial pressure monitoring system. 2018 IEEE International Symposium on Antennas and Propagation & USNC/URSI National Radio Science Meeting, 207–208.
14. **Suzan Miah M, Khan AN, Icheln C, Haneda K and Takizawa K** (2019) Antenna system design for improved wireless capsule endoscope links at 433 MHz. *IEEE Transactions on Antennas and Propagation* **67**(4), 2687–2699.
15. **Basir A and Yoo H** (2019) A stable impedance-matched ultrawideband antenna system mitigating detuning effects for multiple biotelemetric applications. *IEEE Transactions on Antennas and Propagation* **67**(5), 3416–3421.
16. **Gao G, Hu B, Wang S and Yang C** (2018) Wearable circular ring slot antenna with EBG structure for wireless body area network. *IEEE Antennas and Wireless Propagation Letters* **17**(3), 434–437.
17. **Alemaryeen A and Noghanian S** (2019) On-body low-profile textile antenna with artificial magnetic conductor. *IEEE Transactions on Antennas and Propagation* **67**(6), 3649–3656.
18. **Basir A, Bouazizi A, Zada M, Iqbal A, Ullah S and Naeem U** (2018) A dualband implantable antenna with wide-band characteristics at mics and ISM bands. *Microwave and Optical Technology Letters* **60**(12), 2944–2949.
19. **Bouazizi A, Zaibi G, Iqbal A, Basir A, Samet M and Kachouri A** (2019) A dual-band case-printed planar inverted-f antenna design with independent resonance control for wearable short range telemetric systems. *International Journal of RF and Microwave Computer-Aided Engineering* **29**(8), e21781.
20. **Al-Sehemi AG, Al-Ghamdi AA, Dishovsky NT, Atanasova GL and Atanasov NT** (2017) A flexible planar antenna on multilayer rubber composite for wearable devices. *Progress In Electromagnetics Research C* **75**, 31–42.
21. (2006) IEEE standard for safety levels with respect to human exposure to Electric, Magnetic, and Electromagnetic Fields, 0 Hz to 300 GHz. IEEE Std C95.1-2019 (Revision of IEEE Std C95.1-2005/ Incorporates IEEE Std C95.1-2019/Cor 1-2019) 1–312.
22. ICNIR (1998) Guidelines for limiting exposure to time-varying electric, magnetic, and electromagnetic fields (up to 300GHz), ICNIRP. *Health Physics* **74**, 494–522.
23. **Aruna V, Alsath MG, Kirubaveni S and Maheswari M** (2022) Flexible and beam steerable planar UWB Quasi-Yagi antenna for WBAN. *IETE Journal of Research* **68**(3), 2220–2230.
24. **Al-Sehemi A, Al-Ghamdi A, Dishovsky N, Atanasov N and Atanasova G** (2022) Miniaturized wearable antennas with improved radiation efficiency using magneto-dielectric composites. *IETE Journal of Research* **68**(2), 1157–1167.
25. **He K, Gong S and Gao F** (2015) Low-profile wideband unidirectional patch antenna with improved feed structure. *Electronics Letters* **51**, 317–319.
26. **Li ZH, Xue YL, Deng ZQ and Shen T** (2009) Study on optical switching effect of photonic crystals with negative effective index of refraction. *Optik* **120**, 605–609.
27. **Wang J-J, Zhu Z-P, Sun Y-X, Shen T-G and Gong L-L** (2013) Study on left-handed effect of composite helices and its application in squareframe patch antennas. *Optik* **124**, 5189–5192.
28. **Subbaraj S, Kanagasabai M, Alsath MGN, Ganesan G, Panneer Selvam Y and Kingsly S** (2018) Compact multiservice monopole antenna for tablet devices. *International Journal of Electronics* **105**(8), 1374–1387.
29. **Chen J and Zhang A** (2013) A novel design of circularly polarised antenna based on metamaterial. *International Journal of Electronics* **100**(6), 770–778.
30. **Li Y and Li W** (2014) A circular slot antenna with wide tunable and reconfigurable frequency rejection characteristic using capacitance loaded split-ring resonator for UWB applications. *Wireless Personal Communications* **78**, 137–149.
31. **Mishra B** (2019) An ultra-compact triple band antenna for X/Ku/K band applications. *Microwave and Optical Technology Letters* **61**(7), 1857–1862.
32. **Akrou L, Aghzout O, Silva H and Essaaidi M** (2016) Design of compact multiband antenna with band-rejection features for mobile broadband satellite communications. *Progress In Electromagnetics Research C* **68**, 95–106.

https://doi.org/10.1017/S1759078723000454 Published online by Cambridge University Press

33. **Ahsan MR, Islam MT, Habib Ullah M, Aldhaheri RW and Sheikh MM** (2016) A new design approach for dual-band patch antenna serving Ku/K band satellite communications. *International Journal of Satellite Communications and Networking* **34**(6), 759–769.
34. **Sharma M, Kumar Awasthi Y and Singh H** (2017) Planar high rejection dual band-notch UWB antenna with X & Ku-bands wireless applications. *International Journal of Microwave and Wireless Technologies* **9**(8), 1725–1733.
35. **Dalmiya A and Sharma OP** (2016) A novel design of multiband Minkowski fractal patch antenna with square patch element for X and Ku band applications. *International Conference on Recent Advances and Innovations in Engineering (ICRAIE)*, 1–6.
36. **Dawar P, Raghava NS and Asok D** (2015) A novel metamaterial for miniaturization and multi-resonance in antenna. *Cogent Physics* **2**(1), 1–13.
37. **Mishra B, Singh V, Kumar Singh R, Singh N and Singh R** (2018) A compact UWB patch antenna with defected ground for Ku/K band applications. *Microwave and Optical Technology Letters* **60**(1), 1–6.
38. **Ahsan MR, Habib Ullah M, Mansor F, Misran N and Islam T** (2014) Analysis of a compact wideband slotted antenna for Ku band applications. *International Journal of Antennas and Propagation* **2014**, 1–6.
39. **Viswanadha K and Raghava NS** (2021) Design and analysis of a dual-polarization multiband oval ring patch antenna with L-stubs and folded meander line for C-band/X-band/ Ku-band/ K-band communications. *International Journal of Electronics* **108**(4), 647–663.
40. **Reddy VV and Sarma NVSN** (2015) Poly fractal boundary circularly polarised microstrip antenna for WLAN/Wi-MAX wireless applications. *Defence Science Journal* **65**(5), 379–384.
41. **Yang F and Rahmat-Samii Y** (2009) *Electromagnetic Band Gap Structures in Antenna Engineering*. Cambridge: Cambridge University Press.
42. **Ziolkowski RW and Engheta N** (2006) Introduction, history and selected topics in fundamental theories of metamaterials. In Engheta N and Ziolkowski R (eds), *Metamaterials: Physics and Engineering Explorations*, Chapter 1. New York, NY: Wiley.
43. **Caloz C and Itoh T** (2006) *Electromagnetic Metamaterials: Transmission Line Theory and Microwave Applications*. Toronto: John Wiley & Sons.
44. **Priyadarshini J and Jude D** (2019) An investigation on specific absorption rate reduction materials with human tissue cube for biomedical applications. *International Journal of RF and Microwave Computer-Aided Engineering* **29**, 1–19.
45. **Mohamed A, Sharawi M and Muqaibel A** (2018) Implanted dual-band circular antenna for biomedical applications. *Microwave and Optical Technology Letters* **60**, 1125–1132.
46. **Zhang Y, Liu C, Liu X and Zhang K** (2020) A miniaturized circularly polarized implantable RFID antenna for biomedical applications. *International Journal of RF and Microwave Computer-Aided Engineering*, **30**, 1–9.
47. **Mohamed A, Muqaibel A and Sharawi M** (2017) Superstrate loaded miniaturized patch for biomedical telemetry. *Microwave and Optical Technology Letters* **59**(5), 1212–1218.
48. **Zaki A, Hamad E, Abouelnaga T and Elsadek H** (2022) Design of ultra-compact ISM band implantable patch antenna for bio-medical applications. *International Journal of Microwave and Wireless Technologies* **14**(10), 1279–1288.
49. **Pal A, Mishra P and Tripathi V** (2022) A circularly polarized wideband implantable patch antenna for biomedical applications. *International Journal of Microwave and Wireless Technologies*, 1–7.
50. **Ding S, Koulouridis S and Pichon L** (2020) Design and characterization of a dual-band miniaturized circular antenna for deep in body biomedical wireless applications. *International Journal of Microwave and Wireless Technologies* **12**(6), 461–468.
51. **Sievenpiper D, Zhang L, Broas RFJ, Alex¨opolous NG and Yablonovitch E** (1999) High-impedance electromagnetic surfaces with a forbidden frequency band. *IEEE Transactions on Microwave Theory and Techniques* **47**(11), 2059–2074.
52. **Aminian FY and Rahmat-Samii Y** (2003) In-phase reflection and EM wave suppression characteristics of electromagnetic band gap ground planes. *Proceedings of the IEEE International Antennas and Propagation Symposium*, 430–433.
53. **Ali T, Subhash BK and Biradar RC** (2018) Design and analysis of two novel metamaterial unit cell for antenna engineering. *2018 Second International Conference on Advances in Electronics, Computers and Communications (ICAECC)*, 1–4.
54. **Chen X, Grzegorczyk TM, Wu B-I, Pacheco J and Kong JA** (2004) Robust method to retrieve the constitutive effective parameters of metamaterials. *Physical Review E* **70**(1), 016608.
55. **Szabo Z, Park G-H, Hedge R and Li E-P** (2010) A unique extraction of metamaterial parameters based on Kramers–Kronig relationship. *IEEE Transactions on Microwave Theory and Techniques* **58**(10), 2646–2653.
56. **Hosseini M, Klymyshyn DM, Wells G and Liul X** (2014) Thick metal EBG cells with narrow gaps and application to the design of miniaturized antennas. *Progress In Electromagnetics Research* **145**, 185–193.
57. **Elavarasi C and Shanmuganantham T** (2017) CPW-fed SGF-TSRR antenna for multiband applications. *International Journal of Microwave and Wireless Technologies* **9**(9), 1871–1876.
58. **Zhou Y, Zhao N, Ning R and Bao J** (2021) A compact CPW-fed monopole antenna for multi-band application. *International Journal of Microwave and Wireless Technologies* **14**, 1–7.
59. **Jose M, Radha S, Sreeja B, Gulam Nabi Alsath M and Kumar P** (2022) Compact dual-band millimeter-wave antenna for 5G WLAN. *International Journal of Microwave and Wireless Technologies* **14**(8), 981–988.

Saurabh Raj has received his B.Tech degree in Electronics & Communication Engineering from Galgotias College of Engineering and Technology, Greater Noida, Uttar Pradesh, Technical University Lucknow in 2012. He has completed his degree (M.Tech) from BBDNIIT, Lucknow, in 2015. He has completed his Ph.D. from Electronics & Communication Engineering Department from Motilal Nehru National Institute of Technology Allahabad in 2022. His research interests include antenna design for biomedical applications and wireless communication.

Piyush Kumar Mishra has received his B.Tech degree in Electronics and Communication Engineering from Uttar Pradesh Technical University, Lucknow, India, in 2014. He has completed his Master degree (M.Tech) in Electronics Engineering from University of Allahabad, India, in 2019. Currently, he is a research scholar in the Electronics and Communication Engineering Department at Motilal Nehru National Institute of Technology Allahabad, Uttar Pradesh, India. His research interests include antenna design for biomedical applications.

Vijay Shanker Tripathi was born in Gorakhpur (Uttar Pradesh) in 1965. He has completed his Ph.D. from Electronics & Communication Engineering Department from Motilal Nehru National Institute of Technology Allahabad in 2007, M.E. in Digital Systems from Motilal Nehru National Institute of Technology Allahabad in 1999, and B.Tech in Electronics and Telecommunication Engineering from the University of Allahabad in 1988. He is currently the Professor in the Department of Electronics and Communication Engineering, Motilal Nehru National Institute of Technology Allahabad, Prayagraj, and Uttar Pradesh, India. He has authored or co-authored over 60 research papers in international/national journals/conference proceedings. His research interests include RF Circuits and Systems, Antenna, SDR, and Non-Invasive RF Sensors.

https://doi.org/10.1017/S1759078723000454 Published online by Cambridge University Press